Analytical and Experimental Results on System Maximum Reach Increase Through Symbol Rate Optimization

Analytical and Experimental Results on System Maximum Reach Increase Through Symbol Rate Optimization

P. Poggiolini, A. Nespola, Y. Jiang, G. Bosco, A. Carena, L. Bertignono, S. M. Bilal, S. Abrate, F. Forghieri

***Abstract*—We investigated the reach increase obtained through non-linearity mitigation by means of transmission symbol rate optimization (SRO). First, we did this theoretically and simulatively. We showed that the non-linearity model that properly accounts for the phenomenon is the EGN model, in its version that specifically includes four-wave mixing. We then found that for PM-QPSK systems at full-C-band the reach increase may be substantial, on the order of 10%-25%, with optimum symbol rates on the order of 2-to-6 GBaud. We extended the investigation to PM-16QAM, where we found a qualitatively similar effect, although the potential reach increase is typically only about 50% to 60% of that of PM-QPSK. We show that, for C-band PM-QPSK systems over SMF, the potential mitigation due to SRO is greater than that ideally granted by digital back-propagation (the latter applied over a bandwidth of a 32-GBaud channel).**

We then set up an experiment to obtain confirmation of the theoretical and simulative predictions. It consisted of 19 PM-QPSK channels, operating at 128 Gbit/s per channel, over PSCF, with span length 108 km and EDFA-only amplification. We demonstrated a reach increase of about 13.5%, when going from single-carrier per channel transmission, at 32 GBaud, to 8-subcarrier per channel, at 4 GBaud, in line with the EGN model predictions.

***Index Terms*—coherent systems, uncompensated transmission, non-linear effects, GN-model, PM-QAM**

I. Introduction

OVER the last few years, various simulative and theoretical papers [1]-[6] have presented evidence of a dependence of system performance on the transmission symbol-rate. Leveraging such dependence, maximum-reach (MR) or 'Q-factor' gains were found by performing symbol-rate optimization (SRO). The corresponding optimum rates turned out to be substantially lower than the current 32 GBaud industry standard, and typically in the 2 to 6 GBaud range. As for the extent of the MR gains, it was found to be in the 10%–20% range. As for the origin of SRO gains, they were ascribed to peculiar features of fiber non-linear propagation.

Besides theory and simulation, various experimental papers have lately addressed SRO [7]-[11]. Given the low value of the optimum rates, these experiments were conducted by breaking up each single optical channel into subcarriers, generated digitally through the transmitter DSP and DACs. Results on SRO effectiveness were not unanimous. In [7], a 23% MR increase was found when a single 24 GBaud channel was broken up into 8 subcarriers at 4 GBaud. [8] found substantial MR gain in a WDM experiment. However, the gain could also be attributed to other beneficial effects of using subcarriers in that particular set-up. Other WDM experiments [9]-[11] found conflicting results, between about 8% MR gain and no gain at all. Overall, at present, experimental evidence appears to be inconclusive as to the extent of possible SRO gains.

In this paper we try to address the topic of SRO in a comprehensive way. Our first objective was to find an effective NLI modeling framework that could provide a clear picture of the phenomenon and reliable predictions of maximum reach performance, across widely different system scenarios. To this end, we considered three non-linearity models: the GN model [12], the frequency-domain XPM model [13] and the EGN-model [14]. We then carefully checked their predictions vs. detailed simulations. Our results indicate that both the GN and the XPM models are inadequate for addressing this problem. The EGN-model is instead very accurate and is capable of correctly estimating the amount of NLI generated at very different symbol rates, ranging from about 1 to 100 GBaud. This part of the paper expands and refines the preliminary results presented in the conference paper [15].

As a second objective, we wanted to predict the potential benefits of SRO in actual scenarios of interest. Thanks to the EGN model, we could analytically explore a much wider range of scenarios than previously done. In particular, we could push the total system bandwidth to *C-band*, where our results show that the MR gain due to SRO, vs. using the current industry-standard of 32 GBaud, is between 10% and 25%, depending on link features and modulation format. Interestingly, we found that the gain due to SRO appears to be comparable for PM-16QAM, or even greater for PM-QPSK, than what *ideal* digital back-propagation (DBP) can provide, which we estimated using the EGN model to be 10%–15% of MR. We present some preliminary results on combining SRO and DBP and show that there is interesting potential in this respect. We also predict that, using higher symbol-rates than 32 GBaud may actually causes a *loss* of performance. We provide an approximate closed-form analytical formula that accurately estimates the optimum symbol rate. We show that dispersion pre-compensation may have beneficial effects on SRO systems. This part of the paper refines and substantially expands the preliminary results presented in the conference

P. Poggiolini, G. Bosco, A. Carena, Y. Jiang, S. M. Bilal, are with Politecnico di Torino, Dipartimento di Elettronica e Telecomunicazioni (DET), C.so Duca degli Abruzzi 24, 10129 Torino, Italy. Website: http://www.optcom.polito.it, e-mail: pierluigi.poggiolini@polito.it. A. Nespola, L. Bertignono and S. Abrate are with the Istituto Superiore Mario Boella (ISMB), Torino, 10138, Italy (e-mail: nespola@ismb.it; bertignono@ismb.it). F. Forghieri is with Cisco Photonics Italy s.r.l., via Santa Maria Molgora 48C, 20871 Vimercate (MB), Italy. E-mail: fforghie@cisco.com .

paper [16].

As a third objective, we wanted to carry out a carefully designed and controlled SRO experiment to try to provide compelling evidence on whether SRO can actually deliver the predicted gains. We demonstrated transmission of a 19-channel WDM comb over a link using spans of 108 km of PSCF and EDFA-only amplification. We transmitted PM-QPSK over a single-carrier per channel, or either 8 or 16 subcarriers per channel. We found a 12.5% reach increase with respect to the single-carrier case (from 12,620 to 14,180 km), in line with our EGN-model theoretical predictions for the specific scenario. Though further confirmation is certainly needed, this experiment seems to suggest that SRO gains are real. We identify certain specific system and DSP design elements that are highly critical in multi-subcarrier transmission and might explain why other experiments did not find the expected MR or Q-factor gains. This part of the paper is based on the preliminary results presented in the conference paper [17]. With respect to [17], substantially more details are provided on the experiment, the raw acquired samples have been fully reprocessed with new DSP, which has improved results and reduced their spread, and the said elements on system critical aspects have been added. In passing, we would like to mention that our choice of an ultra-long set-up was due to practical experiment implementation reasons. However, link lengths on the order of 15,000 km (or even more) have recently become of interest, after the announcement that the Arctic Fibre project may build the first trans-polar link between Europe and Asia [18].

The paper sectioning follows the three objectives mentioned above. Conclusions follow.

II. Non-Linearity Modeling with SRO

In this section we first try to identify a suitable non-linearity model for the study of symbol rate optimization. We assess model accuracy by comparing model predictions of NLI power with the amount of NLI generated within accurate split-step signal propagation simulations.

Then, we look at system maximum reach performance and we verify that reach predictions, based on the amount of NLI estimated through the model, agree with system simulation results, obtained using split-step link simulations and direct error counting for BER estimation. The details can be found in the following.

A. Testing NLI prediction accuracy

In order to properly study symbol rate optimization, and validate a NLI model for accuracy in this context, a suitable test system layout is necessary. In particular, the per-channel symbol rate R_s should be the free set-up parameter that is probed. All other system features should be kept fixed. To this purpose, we imposed:

1) the modulation format and hence the number of bits per symbol b_s
2) the total optical bandwidth B_WDM
3) the channel spectrum roll-off ρ, assuming a root-raised-cosine spectral shape for the transmitted pulses
4) the *relative* channel spacing $\delta f = \frac{\Delta f}{R_\mathrm{s}}$, where Δf is the channel spacing and R_s is the symbol rate

The above parameters determine the system spectral efficiency and the total (raw) bit rate, which are, respectively:

$$S = \frac{b_\mathrm{s}}{\delta f} \tag{1}$$

$$R_\mathrm{b,tot} = B_\mathrm{WDM} \cdot S \tag{2}$$

Changing the value of R_s affects the number of channels that make up the system, but the key parameters B_WDM, S and $R_\mathrm{b,tot}$ stay the same.

In our NLI model testing campaign we assumed: B_WDM = 504 GHz, ρ = 0.05, δf =1.05, PM-QPSK transmission (b_s = 4). The resulting spectral efficiency and total raw bit rates were S = 3.81 b/(s·Hz) and $R_\mathrm{b,tot}$ = 1.92 Tb/s.

Note that, to avoid inter-channel crosstalk, it must be: $\delta f \geq (1+\rho)$. We selected the smallest δf still ensuring no crosstalk, that is $\delta f = (1+\rho)$. Also, we limited B_WDM to 504 GHz in this first investigation simply to keep simulation time within reasonable bounds. This limitation will be lifted in Sect. III.

As mentioned, R_s was left as the free parameter. There was however one constraint on it. The values of R_s had to be such as to split the WDM bandwidth into a number of channels:

$$N_\mathrm{ch} = \frac{B_\mathrm{WDM}}{(1+\rho)\, R_s} \tag{3}$$

which was exactly an integer number. One of these values is R_s = 32 GBaud, which yields exactly 15 channels.

Regarding link features, we assumed same fiber type in every span and uniform span length L_span in the link. As for the considered fiber types, we chose pure-silica-core fiber (PSCF), standard single-mode fiber (SMF) and non-zero dispersion-shifted fiber (NZDSF). Attenuation was 0.17, 0.22 and 0.22 dB/km, dispersion D was 20.1, 16.7 and 3.8 ps/(nm·km), the dual-polarization non-linearity parameter γ was 0.8, 1.3 and 1.5 $(\mathrm{W{\cdot}km})^{-1}$, respectively. Attenuation was slightly increased with respect to typical spooled values for all fibers, to account for some realistic cabling/splicing loss. The parameters of the NZDSF were chosen similar to Corning's LEAF [19].

We assumed lumped amplification, such as with erbium-doped fiber amplifiers (EDFA), at transparency, i.e., with span loss exactly compensated for by amplifier gain. For SMF and NZDSF we assumed L_span = 100 km, i.e., a typical terrestrial configuration. For PSCF, we assumed a submarine-link design, with L_span = 60 km.

The test set-up described above was then used to generate NLI through simulations. At the link output we measured the NLI power P_NLI falling over the center channel of the WDM comb. Assuming matched filtering at the receiver, and considering the pulse spectrum as approximately rectangular, owing to its small roll-off (0.05), P_NLI is:

$$P_\mathrm{NLI} = \int_{-R_s/2}^{R_s/2} G_\mathrm{NLI}(f)\ df \tag{4}$$

where $G_\mathrm{NLI}(f)$ is the power spectral density (PSD) of the NLI noise. Note that we conventionally assume that the center channel carrier frequency is f=0.

However, P_{NLI} intrinsically depends on both R_s and the launched power per channel so that simply comparing P_{NLI} across systems that use a different symbol rate does not readily provide information regarding the relative maximum reach performance. We therefore derived from P_{NLI} a suitably *normalized* quantity which we called $\tilde{G}_{\mathrm{NLI}}$:

$$\tilde{G}_{\mathrm{NLI}} = \frac{P_{\mathrm{NLI}}}{R_s\, G_{\mathrm{ch}}^3} \tag{5}$$

This quantity can also be viewed as the average value of $G_{\mathrm{NLI}}(f)$ impinging on the center WDM channel, normalized versus the transmitted signal PSD raised to the third power G_{ch}^3. The averaging of $G_{\mathrm{NLI}}(f)$ is carried out by first integrating over the center channel band in Eq. (4) and then dividing by the integration bandwidth R_s in Eq. (5).

The key features of $\tilde{G}_{\mathrm{NLI}}$, are:

- it is independent of the power per channel launched into the link;
- a *same value* of $\tilde{G}_{\mathrm{NLI}}$ among systems using different symbol rates means that the corresponding systems potentially achieve the *same maximum reach.*

The latter feature, in particular, makes $\tilde{G}_{\mathrm{NLI}}$ very convenient for system comparison across different symbol rates.

The simulations were carried out based on a full-band split-step method, as described in detail in [12], Sect. V. The NLI noise was measured on the center channel after subtracting a linearly-propagated version of the signal from the non-linearly-propagated one. The Rx compensated statically for polarization rotation and applied an ideal matched filter. No dynamic equalizer was used, to avoid any possible effect of the equalizer adaptivity on NLI estimation. The simulation was completely noiseless: neither ASE noise, nor any other types of noise, such as Rx electrical noise or laser phase/intensity noise, were present. Simulations were run between 2^{16} and 2^{18} symbols, with fewer symbols at lower symbol rates. The resulting number of simulated samples was therefore in the 5-to-15 millions, across all cases.

Fig. 1 plots the simulation results for $\tilde{G}_{\mathrm{NLI}}$ as markers, when the modulation format is PM-QPSK. The top plot addresses SMF, at 50 spans, the middle plot NZDSF, at 30 spans, and the bottom plot PSCF, at 50 spans. These span numbers for SMF and NZDSF correspond approximately[1] to the system maximum-reach when assuming 32 GBaud symbol-rate, 5 dB EDFA noise figure and BER = $4 \cdot 10^{-3}$. For PSCF, the maximum reach would theoretically be beyond 400 spans, a value too large to simulate in a reasonable amount of time. We therefore decided to curtail the number of PSCF spans to a manageable value of 50. While this does not represent a realistic scenario for PM-QPSK systems, we point out that in this section we are focused on finding an accurate NLI modeling solution, rather than estimating the possible practical advantages of SRO.

[1]These approximate max reach estimates are confirmed by the system simulation results shown later in Fig. 3. They are about 20% lower because the simulations were carried out with an EDFA noise figure of 6 dB, rather than 5 dB. An independent confirmation of the rough estimate of the max reach of about 50 spans over SMF can be found in [21].

The simulation results clearly show the presence of a minimum of $\tilde{G}_{\mathrm{NLI}}$. The related optimum symbol rates are in in general agreement with prior literature [1]-[6].

Regarding the modeling results, the plots show that both the GN-model and the XPM-model fail to reproduce the simulated system behavior, whereas the EGN-model follows it very closely.

Specifically, the GN-model curve is essentially flat, that is, it predicts no change of performance vs. the number of channels (or the symbol rate). This behavior can be traced back to the assumption made in the derivation of the GN-model of the signal behaving as Gaussian noise[2]. While it makes the model very simple, it also makes it miss the dip in NLI shown by the simulations.

The XPM model in its original form [13] does not include single-channel non-linear effects (SCI), so we added the SCI term from the EGN model [14]. The figure shows that XPM (+SCI) tends to be accurate for large symbol rates (low channel count) but it departs very substantially from the simulation results for higher channel count. At the optimum symbol rate, it underestimates $\tilde{G}_{\mathrm{NLI}}$ by about 5 dB for SMF and NZDSF, and about 3 dB for PSCF.

The reason for the behavior of the EGN and XPM (+SCI) models can be better appreciated in Fig. 2, where we plot the detailed breakdown of NLI into its SCI, XPM and FWM components. We show the SMF case, the other two being similar. All three types of NLI contributions are fully accounted for in the EGN model. The EGN model line in Fig. 2 is in fact their sum, that is (SCI+XPM+FWM).

The figure shows that SCI is prevalent at large symbol rate, as it could be expected. Interestingly, in this region SCI and the overall EGN tend to converge to the GN model. At very low R_s, NLI is instead almost completely FWM. Here too, both FWM and the overall EGN tend to converge to the GN model. The middle ground is instead a variable mixture of the three components. However, the figure clearly shows that the optimum symbol rate tends to occur where FWM is prevalent. As a result, the XPM or XPM+SCI models turn out to be completely inadequate for the study of the optimum symbol rate, since they discard FWM. As mentioned, the GN model is inadequate too, although for different reasons, i.e. the signal Gaussianity assumption, which leads to an overestimation of NLI. The EGN model [14] instead fully accounts for FWM and among the tested models is the only one that appears accurate across all symbol rates in Fig. 1. Note that the EGN model had already been found very accurate in various system scenarios at the conventional 32 GBaud symbol rate [14], [20], [21]. Here its accuracy appears to be good over a very wide range of symbol rates as well.

[2]This may be thought of as a viable approximation, albeit a relatively coarse one, under certain constraints. One of these constraints is that the transmitted signals are thoroughly spread out by dispersion. For decreasing values of the symbol rate, however, dispersion becomes less and less effective in doing so and an increasing loss of accuracy of the GN model can be expected, as shown in Fig. 1. The GN model regains accuracy at ultra-low symbol rates (OFDM-like) because the overall signal tends to become 'Gaussian-distributed' due to other reasons. Note that other interpretations of why and when the GN model returns more, or less, accurate results have been proposed, based on a pulse-collision analysis [22].

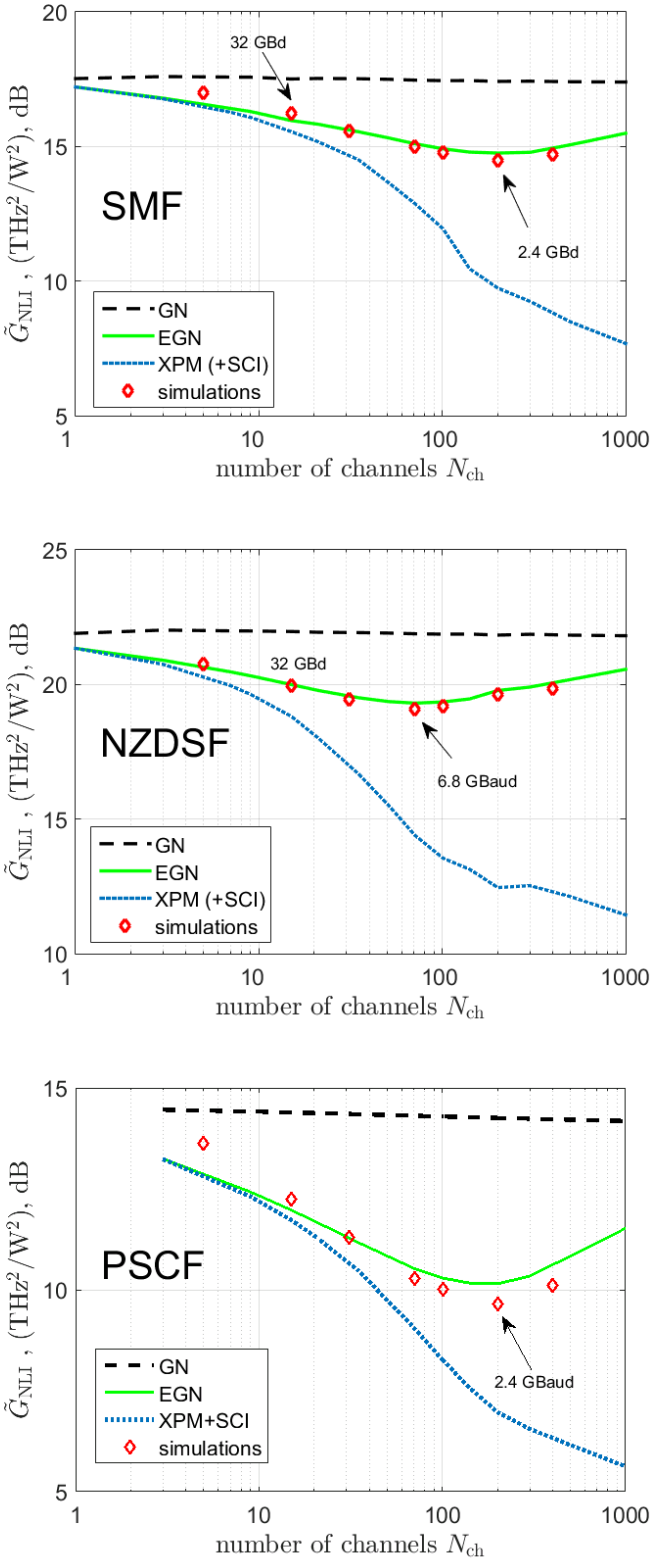

Fig. 1. Normalized average NLI noise power spectral density $\tilde{G}_{\rm NLI}$ over the center channel, vs. the number of channels $N_{\rm ch}$, for a *fixed* total WDM bandwidth of 504 GHz. PM-QPSK modulation, quasi-Nyquist: roll-off 0.05, spacing 1.05 times the symbol rate. NLI is measured at 50 spans of SMF (top), 30 spans of NZDSF (middle) or 50 spans of PSCF (bottom). Lines: calculations using the models indicated in the legend. Markers: dual-polarization split-step simulations.

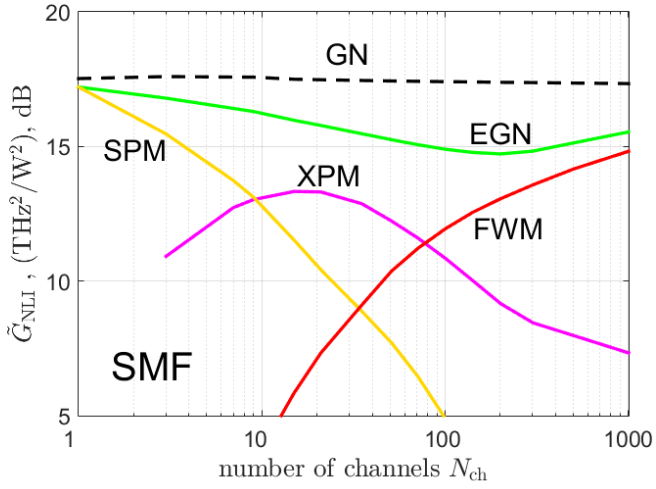

Fig. 2. Same as Fig. 1 (top) but besides the GN and EGN model curves, the individual SPM (also called SCI, for Single-Channel non-linear Interference), XPM and FWM components making up the EGN model curve are shown.

B. Testing system maximum reach prediction accuracy

To verify the accuracy of the EGN model in predicting not just the NLI power but the actual system maximum reach, $L^{\rm max}$, we ran split-step simulations for the same system configurations described in Sect. II-A, at various symbol rates, over SMF and NZDSF. The maximum reach results were obtained through Monte-Carlo simulations with direct error counting. The adaptive equalizer in the receiver, after an initial training-sequence-based initialization was 'frozen' (no longer updated). The same was done for carrier-phase estimation. ASE noise was loaded at the receiver[3].

The analytical estimation of BER, used to predict the reach, was instead based on the non-linear OSNR, calculated as:

$$\mathrm{OSNR}_{\rm NL} = \frac{P_{\rm ch}}{P_{\rm ASE} + P_{\rm NLI}} \tag{6}$$

where $P_{\rm NLI}$ was found using the EGN model and Eq. (4).

Before showing the results, we define the quantity *NLI mitigation* as follows:

$$\Delta\tilde{G}_{\rm NLI,dB} = -10\log_{10}\left(\tilde{G}_{\rm NLI_2}/\tilde{G}_{\rm NLI_1}\right) \tag{7}$$

where the two values of $\tilde{G}_{\rm NLI}$ refer to different number of channels or, equivalently, to different per-channel symbol rates, for the same given total WDM bandwidth $B_{\rm WDM}$. Note that the 'minus sign' in front of the log function is meant to

[3]This was done because our goal was that of validating the EGN model, together with Eq. (6), as an accurate tool for the assessment of the impact of non-linearity on the WDM signal *alone*. This required a benchmark simulation setup which was consistent with the assumption of the presence of the WDM signal only. At any rate, at the chosen system target BER=$4\cdot10^{-3}$, the effect of co-propagating ASE noise is minor [23],[24]. In addition, we are not interested in absolute performance but, rather, in performance variations vs. the symbol rate. Co-propagating ASE noise would then be important only if its contribution to NLI generation was different depending on the system symbol rate. While this is a topic that we deem relevant and worth investigating, we consider it outside of the scope of this paper.

generate a 'positive mitigation' when the numerator is smaller than the denominator. This sign convention is appropriate assuming that the denominator represents a 'reference value' (for instance $\tilde{G}_{\rm NLI}$ at 32 GBaud), while the numerator is an optimized-symbol-rate value to compare the reference with.

Mitigation translates into maximum-reach gain according to the approximate formula [12]:

$$\Delta L^{\rm max}_{\rm dB} \approx \frac{1}{3}\Delta \tilde{G}_{\rm NLI,dB} \tag{8}$$

where Δ represents the ratio of two values of a quantity and $L^{\rm max}$ is the system maximum-reach. For example, a 1 dB NLI mitigation, that is $\Delta\tilde{G}_{\rm NLI} = 1$ dB, can be expected to translate into $\Delta L^{\rm max} = 1/3$ dB, about 8% reach increase.

In Fig. 1, the $\tilde{G}_{\rm NLI}$ minima for SMF and NZDSF are located at about 200 and 70 channels, i.e., at about 2.4 and 6.8 GBaud, respectively. The corresponding NLI mitigation vs. the current industry-standard 32 GBaud (15 channels in the plots) is predicted by the EGN model to be 1.20 and 0.66 dB, respectively. According to Eq. (8), this should lead to 0.4 dB and 0.22 dB (or about 10% and 5%) maximum-reach increase for SMF and NZDSF, respectively.

In all plots of Fig. 1, a simulation marker addresses 96 GBaud transmission too (5 channels), close to those 100 GBaud that are considered as a possible future industry target for transponders aiming at 1 Tb/s throughput. The NLI mitigation between 96 GBaud and the optimum symbol rate is, according to the EGN model, 1.85 and 1.38 dB, resulting in about 15% and 11% predicted reach increase, for SMF and NZDSF, respectively. This shows that $\Delta L^{\rm max}$ is notably larger between the optimum rate and higher values than 32 GBaud.

Coming to the reach results, in Fig. 3 (top and bottom) we show the EGN-model predictions as lines and the simulation results as markers, for SMF and NZDSF, respectively. The overall correspondence is good. In particular, it is very good for low symbol rates. As a whole, they confirm the expected max-reach increase. This means that the NLI curves such as those shown in Fig. 1 do provide a reliable picture of the potential SRO mitigation and that such mitigation does translate into max-reach gains as expected.

In conclusion of this section, we have identified a suitable NLI analytical model, the EGN model, that appears to account quite well for the NLI variability vs. the symbol rate, correctly predicting the simulated NLI noise variance and system reach over different fiber types. In the following, we will use this analytical model as the basis for obtaining predictions of SRO mitigation and MR gains in system scenarios of practical interest. In particular, we will push the explored WDM bandwidth to C-band and we will include PM-16QAM.

III. Probing SRO effectiveness

A. C-band systems

Fig. 4-(top) shows the normalized average NLI noise power spectral density $\tilde{G}_{\rm NLI}$ at 50 spans of SMF assuming PM-QPSK transmission, with the same system parameters as used for Fig. 1-(top). The total WDM bandwidth $B_{\rm WDM}$ is however ramped up from 500 GHz to 1.5, 2.5 and 5 THz (C-band). Notice that the abscissa is now the symbol rate per channel R_s,

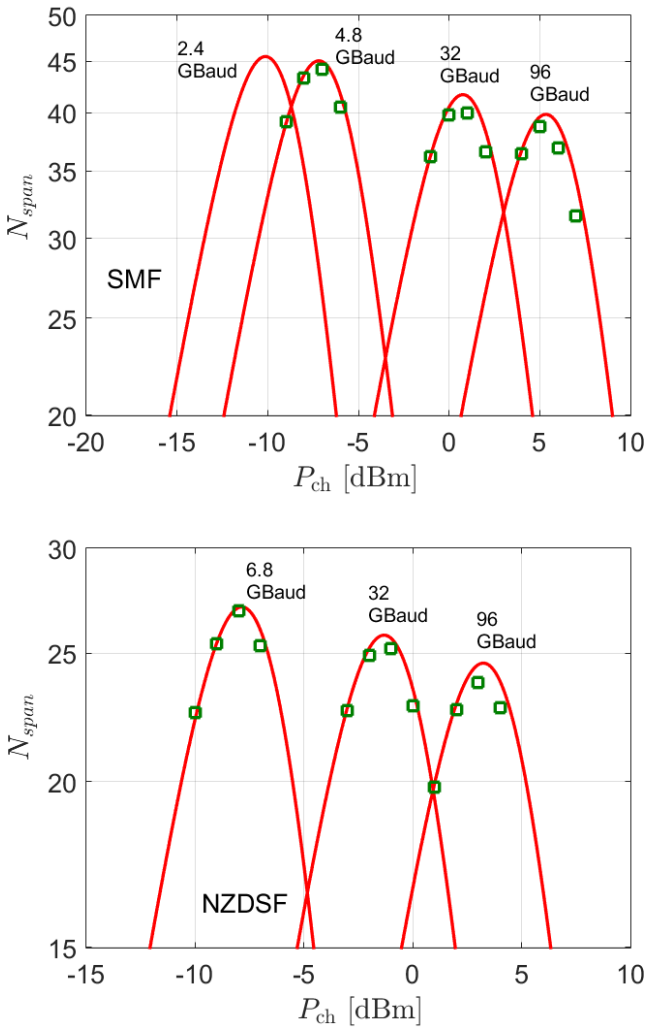

Fig. 3. Reach curves at BER=$4\cdot10^{-3}$ vs. launch power per channel. Parameters: PM-QPSK, roll-off 0.05, spacing $1.05\cdot R$, $L_{\rm span}$=100 km, EDFA noise figure 6 dB. Solid lines: EGN-model predictions. Markers: simulation results. Top plot: SMF. Bottom plot: NZDSF.

rather than the number of channels. The relationship between the two is provided by Eq. (3). The solid curves are obtained using the EGN model and the lowest one is the same as shown in Fig. 1-(top) for $B_{\rm WDM}$ 500 GHz, reproduced here as baseline, together with the corresponding simulations.

The general shape of all the curves remains unchanged for the different values of $B_{\rm WDM}$ and, in particular, the optimum symbol rate does not change. However, the NLI mitigation, between the current industry standard (32 GBaud) and the optimum rate, goes up as $B_{\rm WDM}$ is increased. At C-band it is about 1.8 dB, up from about 1.3 dB at 500 GHz. We tried to back up this finding by extending the simulations to at least $B_{\rm WDM}$= 1.5 THz. We show three data points (red 'x' markers) that, although slightly higher (0.15 to 0.25 dB) than the analytical curve, indicate the same amount of SRO mitigation as the curve, between 32 GBaud and the optimum rate. We tentatively attribute the NLI overestimation of the simulations to some loss of accuracy of the split-step algorithm

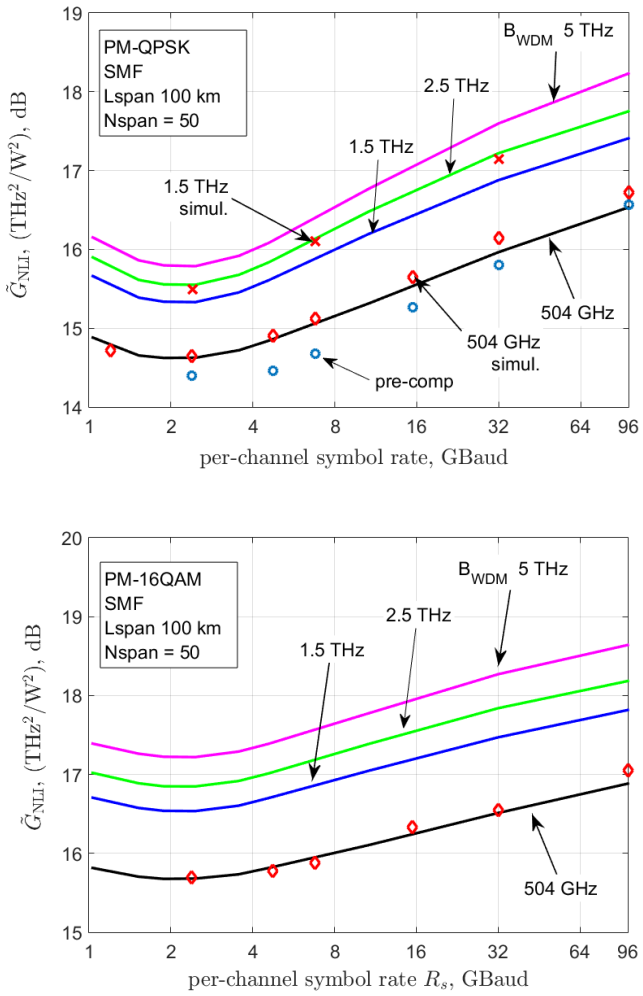

Fig. 4. Normalized average NLI noise power spectral density $\tilde{G}_{\rm NLI}$ over the center channel, vs. the symbol rate per channel R_s, for four WDM bandwidth values: 0.5, 1.5, 2.5 and 5 THz (C-band). NLI is measured at 50 spans of SMF. Roll-off is 0.05, channel spacing $1.05{\cdot}R_s$. Top: PM-QPSK modulation. Bottom: PM-16QAM. Solid lines: calculations using the full EGN model. Markers: dual-polarization split-step simulations: diamonds for 0.5 THz, 'x' markers for 1.5 THz, circles 0.5 THz with dispersion pre-compensation (see Sect. III-F).

at these large bandwidths.

Pending further necessary simulative and experimental confirmation, this first indication that SRO does not lose effectiveness when $B_{\rm WDM}$ is increased, as opposed for instance to DBP, is quite significant, in view of practical applications.

B. SRO and PM-16QAM

We also extended the investigation to PM-16QAM. Fig. 4-(bottom) shows the results, assuming the same system layout and parameters as for Fig. 4-(top). We chose to measure again NLI at 50 spans, to allow a direct comparison with the PM-QPSK results. Note that 50 spans would still be close to the system maximum reach, if assuming hybrid EDFA-Raman amplification and about 10^{-2} as target BER[4].

The PM-16QAM simulations for $B_{\rm WDM}$= 504 GHz (diamond markers) are shown together with the EGN model curves (solid lines).

NLI mitigation due to SRO is still clearly present, though its extent is smaller than for PM-QPSK. At C-band it is about 1.15 dB, between 32 GBaud and the optimum symbol rate. Interestingly, the latter is still the same as that of PM-QPSK, about 2.4 GBaud.

C. Comparison between PM-QPSK and PM-16QAM

Regarding max-reach, according to Eq. 8 the mitigation of $\tilde{G}_{\rm NLI}$ due to SRO for the systems of Fig. 4 can be expected to lead to a 15% and 9% max-reach increase for PM-QPSK and PM-16QAM, respectively, *at C-band*, vs. the 32 GBaud systems.

We also found a good match between the $\tilde{G}_{\rm NLI}$ EGN-model predictions and simulation results for PM-16QAM, at $B_{\rm WDM}$= 504 GHz, for 30 spans of NZDSF with $L_{\rm span}$= 100 km, and 50 spans of PSCF with $L_{\rm span}$= 60 km. The respective EGN-model NLI mitigation, estimated at *C-band,* between 32 GBaud and optimum rate, are:

PSCF, 60 km spans:
PM-QPSK 2.1 dB; PM-16QAM 1.07 dB

NZDSF, 100 km spans:
PM-QPSK 1.1 dB; PM-16QAM 0.64 dB

Note that, as a rule-of-thumb, a ratio of PM-16QAM vs. PM-QPSK mitigation (in dB) of about 50% to 60% is typically observed, all other parameters being equal.

D. Penalty increasing the symbol rate

The industry appears to be very keen on increasing the per-channel throughput and one obvious way to do it is by ramping up the symbol rate. Our results show, however, that NLI is enhanced when going to higher rates, albeit not dramatically. From Fig. 4 (top), the NLI gap between the optimum rate and 96 GBaud, at C-band, amounts to a hefty 2.44 dB, or about 21% of reach. Compounding the intrinsic technological difficulty of achieving 64 or 96 GBaud with further fundamental NLI penalty may eventually create a disincentive towards obtaining higher rates in a single-carrier configuration. For this, and perhaps other technology-related reasons, it may be that higher throughput channels will actually consist of a multiplex of lower-rate subcarriers.

[4]In [21] a similar PM-16QAM link was found both by simulation and EGN model to achieve 11 spans with EDFA noise figure (NF) 6 dB, at target BER $4 \cdot 10^{-3}$. Raman would not substantially alter NLI if backward-pumped and delivering no more than 14-15 dB gain, over the assumed 22-dB span loss [25]. In these conditions, about 6-7 dB of noise figure can be gained [25]. Increasing the target BER to 10^{-2} and applying a 7 dB noise figure reduction, a 50-span max reach is found through Eq. 59 in [12].

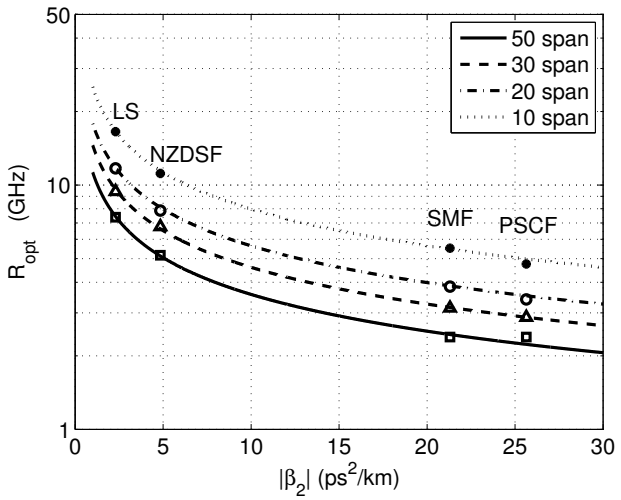

Fig. 5. Value of the optimum symbol rate as predicted by Eq. 9 (solid lines) or by the EGN-model (markers), as a function of fiber dispersion and of link length in number of spans ($L_{\rm span}$=100 km).

E. Closed-form optimum symbol-rate formula

We obtained a closed-form approximate expression of the optimum symbol rate, by using results from the derivation of the asymptotic closed-form EGN model proposed in [20]. For quasi-Nyquist systems like the ones considered in this paper, with all identical spans, the optimum rate is:

$$R_{\rm opt} = \sqrt{2/(\pi\,|\beta_2|\,L_{\rm span}\,N_{\rm span})} \tag{9}$$

We show in Fig. 5 an extensive test of Eq. (9), carried out over a WDM bandwidth of 504 GHz. The markers are drawn by finding the optimum symbol rates from complete EGN-model $\tilde{G}_{\rm NLI}$ curves like those of Fig. 1 for the same PM-QPSK WDM transmission signal used there. The solid lines are Eq. (9). The plot shows an excellent match, vs. the wide range of dispersions and number of spans addressed. In addition, we tested a few data points for $L_{\rm span}$= 50 and 60 km, over SMF and PSCF. In these cases too Eq. (9) proved accurate. The LS fiber, not previously introduced in this paper, had parameters: attenuation 0.22 dB/km, dispersion $D = -1.8$ ps/(nm·km), non-linearity parameter $\gamma = 2.2$ (W·km)$^{-1}$, respectively.

The formula indicates that the optimum rate is a function not only of the accumulated dispersion per span $|\beta_2|\cdot L_{\rm span}$ but also of the link length through $N_{\rm span}$. This actually agrees with a prior simulative indication from [3]. Owing to the square root in Eq. (9), the range of optimum rates is relatively narrow. It goes above 10 GBaud only for LS fibers and for relatively short NZDSF links.

Note that the formula does not depend on either the transmission format nor the total WDM bandwidth. We did not extensively check for these feature of $R_{\rm opt}$, but indeed Fig. 4 shows essentially no change of optimum rate when either enlarging $B_{\rm WDM}$ or changing format between PM-QPSK and PM-16QAM. We observed format-independence in other test-cases too, such as PSCF with 60 km spans and NZDSF with 100 km spans, mentioned in Sect. III-C.

The optimum rate formula is derived by imposing $f_1 = R_s/2$ in Eq. (27) of [20]. The latter formula can be thought of as identifying a peculiar frequency such that, when the symbol rate approaches it, the XPM contribution to NLI rapidly falls off (see discussion of the properties of the function μ^a in the appendix of [20]), to be replaced by FWM. The speed of decrease of XPM is not matched by the growth of FWM, giving rise to a local NLI minimum, as clearly visible in Figs. 1-2. It is this circumstance that brings about SRO mitigation.

Eq. (9) can be extended to non-Nyquist-WDM systems, yielding:

$$R_{\rm opt} = \sqrt{\frac{2}{\pi\,|\beta_2|\,L_{\rm span} N_{\rm span}\,(2\,\delta f - 1)}} \tag{10}$$

where $\delta f = \Delta f / R_s$ is the normalized channel frequency spacing.

F. The effect of dispersion pre-compensation

Dispersion pre-compensation (DPC) can provide some NLI mitigation benefit [26]. We tried to combine DPC and SRO on the 50-span SMF PM-QPSK system, with 100 km span length, that we have repeatedly used as test set-up in this paper. The amount of dispersion pre-compensation that we applied was half of the total link accumulated dispersion, as recommended in [26]. The results are shown as circle markers in Fig. 4 (top). Although they should be considered as preliminary, they appear to show that some further NLI mitigation can be obtained, vs. SRO alone. In addition, the same amount of NLI mitigation that is found at the optimum symbol rate (about 2.4 GBaud) with SRO only, can also be obtained with DPC+SRO at about 7 GBaud. This may be beneficial since, even assuming DAC-supported subcarrier multiplexing, it may be problematic to implement symbol rates as low as 2 GBaud, or less. Also, the very long symbol times related to very low symbol rates may make practical systems more vulnerable to phase noise, or otherwise require more sophisticated phase-noise mitigation DSP.

It should be noted that pre-compensation may increase the peak-to-average power-ratio (PAPR) of the electrical signals in the Tx, leading to more stringent requirements on Tx component performance, such as for instance the DACs ENOB (effective number of resolution bits). On the other hand, if SRO is implemented through electrical subcarrier multiplexing, the PAPR is already enhanced by it and the addition of pre-compensation should not substantially worsen it.

In other words, the PAPR problem must be dealt with anyway for multi-subcarrier SRO implementation and in that context the addition of pre-compensation should not result in substantial penalties.

G. SRO and digital back-propagation

We carried out a comparative study of SRO vs. digital back-propagation (DBP) using the EGN model, on a test-system configuration consisting of 32-GBaud WDM channels, spaced 33.6 GHz. The modulation format was either PM-QPSK or

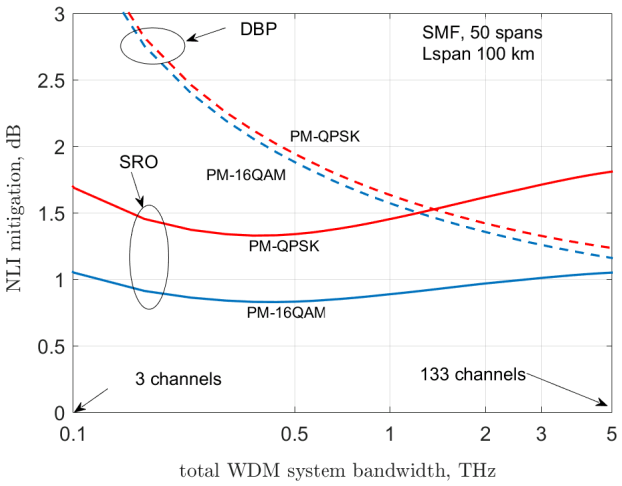

Fig. 6. NLI mitigation vs. total system WDM bandwidth for SRO and DBP. Transmission is quasi-Nyquist, roll-off 0.05, spacing $1.05{\cdot}R_s$. For DBP the symbol rate R_s is 32 GBaud. For SRO it is close to the optimum symbol rate (about 2.3 GBaud). NLI mitigation is measured vs. conventional transmission at 32 GBaud.

PM-16QAM. The number of channels was varied from 3 to 133, corresponding to a total system WDM bandwidth $B_{\rm WDM}$ spanning between 100 GHz and 5 THz (C-band). The link consisted again of 50 spans of SMF, with span length 100 km. SRO consisted of transmitting each 32-GBaud WDM channel as 14 subcarriers at 2.286 GBaud. This value is very close to the optimum rate for this system, which is about 2.4 GBaud, independently of the WDM bandwidth, as shown in the previous sections. DBP was assumed completely ideal, carried out over the whole receiver optical bandwidth of 33.6 GHz. Spectra were raised-cosine with roll-off 0.05, both for single-carrier and multi-subcarrier. Subcarriers did not overlap.

In Fig. 6 the theoretical NLI mitigation is shown, measured vs. conventional transmission (using neither SRO nor DBP) at 32 GBaud. Fig. 6 clearly confirms the well-known decrease of effectiveness of DBP vs. WDM bandwidth (see sect. IX of [12]). SRO, on the contrary, shows a C-band value that is comparable to the 3-channel value. SRO effectiveness actually has a dip at about 400 GHz of WDM bandwidth. Both the dip and the subsequent increase of mitigation, as well as the actual mitigation values at 500 GHz and 1.5 THz, agree well with the simulation results shown in Fig. 4. At C-band, the DBP mitigation is 1.25 dB for PM-QPSK and 1.15 dB for PM-16QAM. In other words, SRO outperforms ideal DBP with PM-QPSK, whereas SRO and ideal DBP are almost equivalent with PM-16QAM.

Note that actual DBP mitigation can be expected to be smaller than the ideal numbers reported above. In particular, apart from possible computational DSP limitations, DBP is known to be vulnerable to polarization effects such as PMD [27] and to co-propagating ASE noise [24]. Of course SRO too could be vulnerable to these or other factors that are not accounted for in the EGN model calculations. The experiment reported on in Sect. IV however provides substantial evidence towards SRO delivering mitigation which is rather close to ideal. Since NLI mitigation due to SRO and DBP is based on quite different mechanisms, it is possible that their benefit might add up. If so, then max-reach gains in the 20% to 30% range might be feasible, depending on how effectively the two techniques combine. We believe this is an interesting topic for possible future research. Preliminary results will appear in a forthcoming paper devoted to further investigating this aspect [37].

H. Impact of non-linear phase-noise

The NLI power results shown in Figs. 1 and 4 are not selective, in the sense that they show the total NLI power, irrespective of it possibly being classifiable as 'non-linear phase-noise' (NLPN). Since the EGN model is not selective either, these figures are internally consistent.

Several papers have recently addressed the topic of non-linear phase noise (NLPN), both theoretically [28]-[33] and experimentally [34], [35]. Both theory and experiments indicate that NLPN is quite modest in lumped-amplification long-haul systems using PM-QPSK, whereas it may have a non-negligible presence in similar PM-16QAM systems. Distributed amplification enhances NLPN, but significantly so only when it approaches ideal distributed amplification. Specifically, hybrid amplification, which splits loss compensation between a Raman amplifier and an EDFA, do not typically enhance phase noise.

One of the key features of NLPN is that it shows up as a long-correlated noise component, with time-correlation steadily increasing vs. accumulated link dispersion. This circumstance has been clearly shown also experimentally [34], [35]. For this reason, NLPN is typically thoroughly removed by conventional CPE algorithms that are present in typical Rx DSP to deal with conventional laser phase-noise, as shown in [35].

In this paper we are interested in NLPN to the extent that it might alter some of the conclusions on SRO, otherwise reached without considering its impact. To this goal, we looked at the features of NLI in particular at 32 GBaud and at 2.4 GBaud, in the PM-QPSK and PM-16QAM systems of Fig. 4. We used the technique proposed in [32] and also used in [34], [35], which consists of bringing each constellation point onto a single one, in such a way that the locally tangent and radial axes to each constellation point become aligned. We then looked at the correlation features of noise on such tangent and radial axes, to be able to detect NLPN reliably.

Our results show that NLPN is small for the PM-QPSK data points, and long-correlated. When ideally removed, in a way similar to the 'PN-receiver' in [34], the total amount of NLI power decreases by about 0.2 dB. This decrease is the same at 2.4 and 32 GBaud which suggests that, at least in the probed scenario, it would not alter our conclusions on potential SRO gains.

When looking at PM-16QAM simulations, we found a substantially larger amount of NLPN. When removed, again the 2.4 and 32 GBaud simulation points shifted downward,

both by about 0.6 dB[5]. This shift may have some detectable impact on overall performance prediction (about 4% of max-reach) but, again, being the same for both rates, it would not alter the predictions on potential SRO gains.

As a word of caution, removing NLPN in an actual PM-16QAM systems at very low symbol rates may require ad hoc non-standard algorithms, since the NLPN correlation, albeit long in absolute terms, may amount to only a few symbol times when operating at low-GBaud symbol rates.

IV. Experimental Test of SRO Effectiveness

Theoretical and simulative predictions of any effect or phenomenon can provide an indication of its *possible* occurence, but then reliable experimental confirmation needs to follow. However, as discussed in the introduction, SRO experiments have so far yielded rather conflicting results (see Sect. I for details).

To obtain a firmer experimental confirmation of SRO merits, we carried out a specifically devoted experiment. The high-level set-up features are as follows. The system consisted of 19 WDM channels, spaced 37.5 GHz. The transmission format was PM-QPSK. The total symbol rate for each channel was 32 GBaud. Each channel was transmitted as *either* single-carrier at 32 GBaud *or* multi-subcarrier (multi-SC). In the multi-SC case, each channel was subdivided into either 8 or 16 subcarriers, with per-SC symbol-rate of 4 and 2 GBaud, respectively. The link consisted of a re-circulating loop with four spans of PSCF, with average span length 108.2 km and EDFA-only amplification.

Despite the long span-length and the use of lumped-only amplification, the max-reach exceeded 13,000 km in even the least favorable of the tested configurations. We would like to point out that our choice of such ultra-long-haul set-up was due lab equipment constraints and to SRO mitigation being more substantial and hence more easily detectable in this scenario. However, link lengths on the order of 15,000 km (or even more) have recently become of interest, after the announcement that the Arctic Fibre project might build the first trans-polar link between Europe and Asia [18]. Also, links exceeding 12,000 km are already under construction.

In the following, the details of the set-up will be provided.

A. Test set-up detailed description

The schematic of the experiment is shown in Fig. 7. An array of 19 lasers (192.349 to 193.024 THz) was arranged at 37.5 GHz frequency separation. The channel under test (CUT), at the center of the comb, was generated using an external-cavity laser (ECL). For all interfering channels, DFB lasers were used. A pair of single-nested Mach-Zehnder modulators created the odd and even interfering carriers. Polarization multiplexing (PM) of the interfering channels (INTs) was obtained through a PM emulator. The CUT signal was directly generated as PM by a *double*-nested Mach-Zehnder modulator.

Spectral shaping was applied to the single-carrier or to each SC through DSP in order to obtain raised-cosine spectra with roll-off 0.05. In order to avoid inter-SC crosstalk, the SC frequency spacing was set to $1.05 \cdot R_{\mathrm{sc}}$, where R_{sc} is the subcarrier symbol rate. The combined multi-SC signal was digitally pre-emphasized to compensate for in-band bandwidth limitations of the transmitter (Tx) components. The digital single-carrier or multi-SC signals were converted into analog signals using programmable CISCO prototype DACs running at 64 GSamp/s. Due to DAC memory constraints, different PRBS lengths were used: 2^{15}-1 for the single-carrier signals and 2^{11}-1 for the multi-SC ones. Independent PRBSs were used for each SC *within* the CUT, the odd INTs and the even INTs. PRBSs were also different *between* CUT, odd and even INTs. Broad-band RF amplifiers were used to increase the peak-to-peak amplitude voltage to about 25% of the modulator V_π. A plot of the electrical spectrum of the signal for the x-polarization at the input of the CUT modulator is shown in Fig. 8.

A dispersion-uncompensated transmission link was implemented as a re-circulating loop consisting of four spans of PSCF, with average length and loss equal to, respectively, 108.2 km and 18.75 dB. Each of the four spans actually consisted of two different types of PSCF, as shown in Table I.

Notice that the larger effective-area sections were placed first in each span. Fiber data was supplied by the fiber manufacturer (SEI). The loop made use of EDFA-only amplification and included a spectrally-resolved gain equalizer

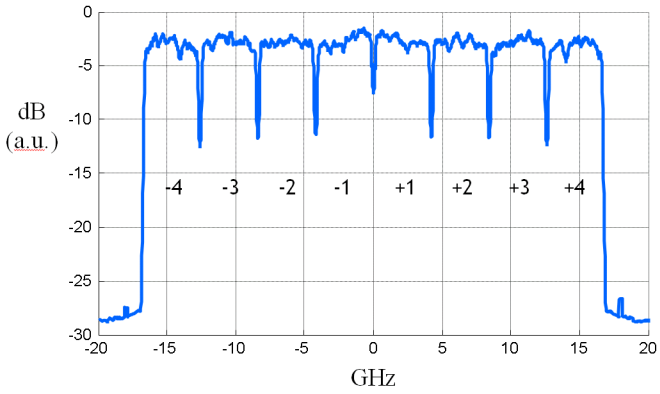

Fig. 8. Power spectrum of the electrical signal for the x-polarization at the input of the Mach-Zehnder modulator for the channel under test, in the case of transmission with 8 subcarriers at 4 GBaud. The subcarrier labeling that we used is shown in figure, ranging from -4 to +4 (skipping '0')..

span #	first section	second section
span 1	$\approx$ 54km, 150 μm^2	$\approx$ 54km, 110 μm^2
span 2	$\approx$ 54km, 150 μm^2	$\approx$ 54km, 110 μm^2
span 3	$\approx$ 54km, 130 μm^2	$\approx$ 54km, 80 μm^2
span 4	$\approx$ 54km, 130 μm^2	$\approx$ 54km, 80 μm^2

TABLE I
Span sections with fiber lengths and effective areas

[5]In [16] we erroneously wrote that NLPN removal was necessary to bring the simulated $\tilde{G}_{\mathrm{NLI}}$ points for PM-16QAM down onto the EGN model predictions. Otherwise they would have been 0.6 dB higher. We later found that a simulation accuracy parameter had been erroneously set, generating fictitious excess NLI. We re-ran all the simulations for this paper and found that the $\tilde{G}_{\mathrm{NLI}}$ simulation points are in quite good agreement with the EGN-model theoretical curve, without NLPN removal, as it should in fact be the case.

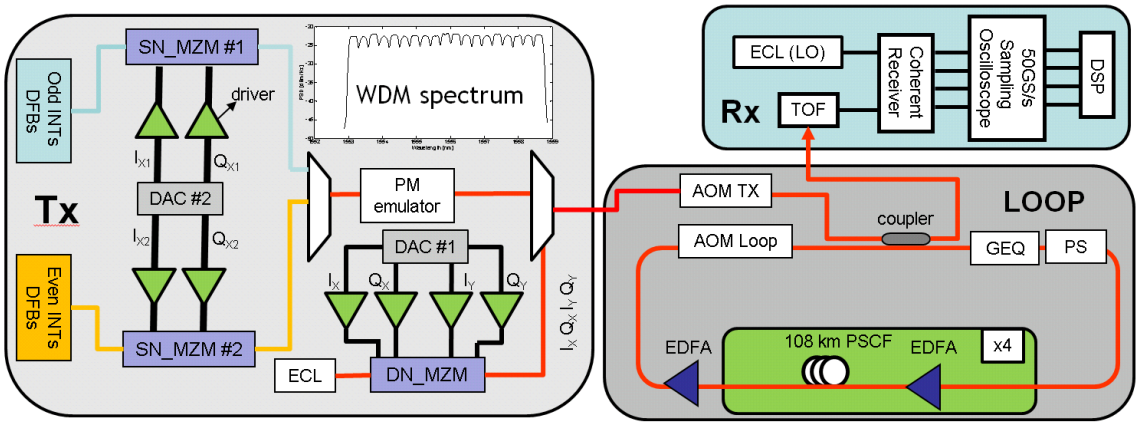

Fig. 7. Schematic of the experimental SRO test set-up. Legenda. INT: interfering channels (not the channel under test). SN_MZM: single-nested Mach-Zehnder modulator. DN_MZM: dual-nested Mach-Zehnder modulator. GEQ: gain equalizing programmable filter. PS: loop-synchronous polarization scrambler. AOM: acousto-optic modulator (used as switch). TOF: tunable optical filter.

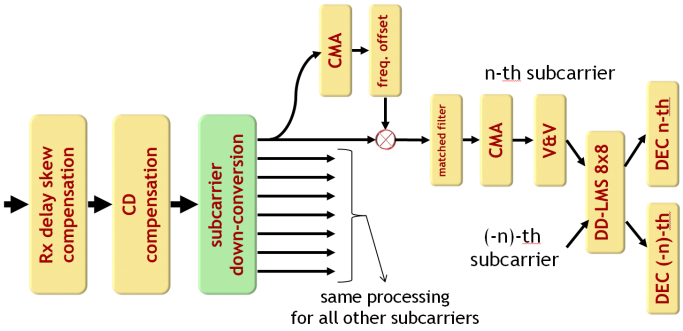

Fig. 9. Block diagram of the receiver DSP, for the case of multi-subcarrier transmission, with 8 subcarriers. All subcarriers are processed independently till the last 8x8 equalizer stage, where the signals after V&V from the n-th and $(-n)$-th subcarriers (those symmetric vs. the channel center frequency) converge, for joint processing.

channel structure	2x2 CMA taps	V&V taps	8x8 LMS taps
1SC @ 32 GBaud	81	100	81
8SC @ 4 GBaud	21	100	81
16SC @ 2 GBaud	21	90	51

TABLE II
NUMBER OF TAPS OF VARIOUS DSP STAGES.

(GEQ) and a loop-synchronous polarization scrambler (PS) to, respectively, compensate for the EDFA gain-tilt and ripples and to effectively average the impact of polarization effects. An additional fifth EDFA was used to compensate for the insertion loss due to the GEQ, PS, couplers and acousto-optic modulators.

At the receiver (Rx) side, the signal was mixed with an ECL local oscillator (LO), then sampled and recorded by a 50 GSamp/s real-time scope operated at 16 GHz baseband bandwidth (Tektronix DPO73304DX). The acquired signals were re-sampled at 64 GSamp/s, then Rx DSP was applied (see Fig. 9). First, compensation of the I/Q imbalance (different amplitude and skew) introduced by the Rx front-end was applied. Compensation of CD followed. In the case of multi-SC signals, a frequency down-shift stage then converted each separate SC to baseband. From this point on, each subcarrier was processed independently.

First, possible residual subcarrier frequency-offset was eliminated by means of a fine-frequency-offset estimator, fed by a dedicated 2x2 complex-valued butterfly adaptive equalizer, driven by a constant modulus algorithm (CMA). Notice that the signal produced by this CMA stage was *not* used for demodulation, it only served as input to the frequency offset estimator. After residual frequency-offset compensation, matched filtering took place, followed by another CMA-driven 2x2 complex-valued butterfly adaptive equalizer stage, which took care of MIMO de-muxing and further fine equalization. Then, phase-noise was mitigated by means of a Viterbi-and-Viterbi carrier phase estimator (CPE).

If the in-phase (I) and quadrature (Q) signals were ideal, frequency down-conversion and baseband filtering would be sufficient for isolating each individual subcarrier. On the other hand, time-skew and gain imbalance between the I and Q components break this ideality and cause mutual interference between each pair of symmetric subcarriers. These are those subcarriers positioned at frequencies symmetric with respect to the channel center frequency, or equivalently, at indices $\pm n$ according to the labeling system of Fig. 8. Such crosstalk cannot be canceled out by any equalizer operating on each subcarrier alone, neither by a 2x2 complex-valued equalizer nor by a 4x4 real-valued one. This may induce a significant penalty on the multi-SC system performance, which is actually worse for the subcarriers that are further away from the channel center frequency.

Three countermeasures were taken in order to eliminate this penalty: suitable hardware calibration was performed for the compensation of the I/Q skew and imbalance introduced by the Tx devices; a digital delay de-skew technique was applied as the first stage of the Rx DSP (as mentioned); and a final 8x8 real-valued butterfly equalizer was added as the last processing block, which jointly processes two frequency-symmetric subcarriers (those with index $\pm n$), each represented by four real signals. The use of the 8x8 stage was particularly beneficial and completely solved the problem. In fact, the subcarriers farther away from the center channel frequency,

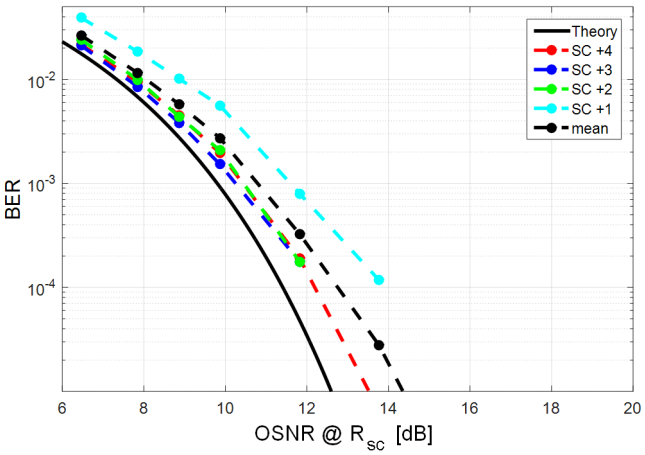

Fig. 10. Back-to-back BER vs. OSNR for the 8-subcarrier system. The curves shown refer to subcarriers +1 to +4 (see Fig. 8 for the meaning of the numbering). The OSNR bandwidth is referred to the per-subcarrier symbol rate of 4 GBaud.

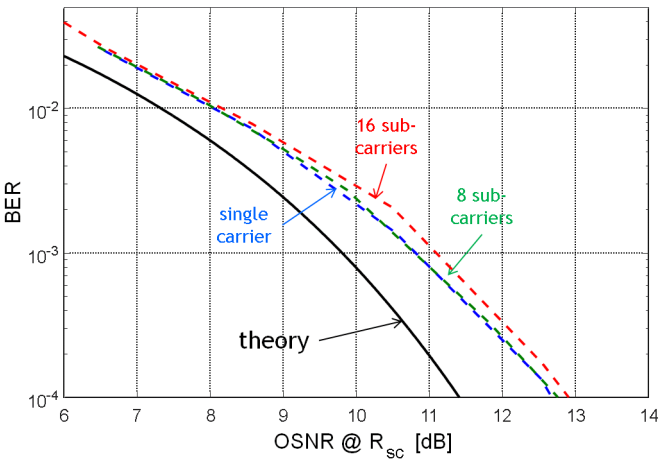

Fig. 11. Back-to-back BER of the channel under test, vs. OSNR, for the single-carrier, 8-SC and 16-SC cases. The OSNR bandwidth is referred to the per-subcarrier symbol rate.

which were the worst performing, turned out to be the ones with lower BERs, as discussed below.

The number of taps used in the 2x2 CMA equalizer, V&V CPE and the 8x8 real LMS equalizer are shown in Table II. They were optimized, in any case, performance did not change significantly over relatively large tap number intervals.

Fig. 10 shows, for the 8-SC case, the individual BERs of the subcarriers +1 through +4. Those of the corresponding negative indices were very similar. Note that OSNR is defined over a bandwidth equal to R_{sc}, that is, 4 GHz. The plot shows that by far the worst performing subcarrier was the one closest to the channel center frequency. The best performing were +3 and +4, the furthest away from it. We investigated the matter and found that the DAC suffered from some amount of non-linear response, which created non-linear subcarrier crosstalk products at low frequencies, which superimposed with the subcarriers ± 1 and somewhat degraded them.

Fig. 11 shows the overall back-to-back BER results for the CUT, vs. the optical signal-to-noise ratio (OSNR), for the single-carrier, 8-SC and 16-SC cases. In the multi-SC case, BER was obtained as the average over all the individual SCs making up the CUT. The OSNR penalty with respect to theory at the target BER of 10^{-2} was 0.7 dB, identical for the single-carrier and 8-SC cases. It was about 0.11 dB worse for the 16-SC case. Interestingly the mean value of the individual subcarrier BERs shown in Fig. 10 actually led to an overall BER that coincided with that of the single-carrier case.

The results of the propagation measurements are shown in Fig. 12, in terms of reach in number of spans N_{span} as a function of the launched power per SC, at BER = 10^{-2}. Three data points are shown per launch power, corresponding to successive measurements. Repeatability was very good, with the exception of the 16-SC case that showed increased variability.

The single-carrier system reached about 116 spans, or 12,550 km. The 8-SC system reached about 132 spans, or about 14,280 km, achieving a max-reach increase of about 13.7% with respect to the single-carrier case. The 16-SC system slightly under-performed with respect to the 8-SC system, reaching about 130 spans, or a 12% reach increase vs. single-carrier.

The predictions obtained using the EGN-model are shown as solid lines in Fig. 12. They take into account the btb performance of the different set-ups. The effect of co-propagating ASE noise and channel power depletion were taken into account too, as proposed in [23]. The equivalent EDFA noise figure (5.2 dB) used in the EGN-model predictions was estimated by matching the performance of the single-carrier system when operating in the linear regime. No further fitting was performed to generate the multi-SC prediction. The correspondence between measured and EGN-model max-reach increase predictions is therefore good. Note that experimental parameter estimation errors may be present, but the reach *increase* prediction should be robust vs. such errors.

The 16-SC system fell somewhat short of the predictions, albeit it still delivered substantial reach increase. At present we have no firmed-up explanation for this behavior. In particular, we do not know whether it should be ascribed to implementation impairments or to other effects.

B. Comments on the experimental results

In view of the somewhat conflicting reports from various groups, our experiment was meant to try and provide some firm evidence regarding the effectiveness of the SRO concept, or otherwise lack thereof.

Our assessment of the results is that our set-up performed very close to the theoretical SRO gain predictions, at least in the 8-SC case, with the 16-SC falling somewhat short, but still delivering substantial performance gain. In our opinion, this experiment provides still partial, but somewhat compelling evidence that SRO can provide max-reach gains close to the extent predicted by theory.

We did however learn that certain implementation details are critical, which might perhaps help explain some of the conflicting results obtained by other experiments. In particular, the I/Q delay skew is extremely critical and even conventional

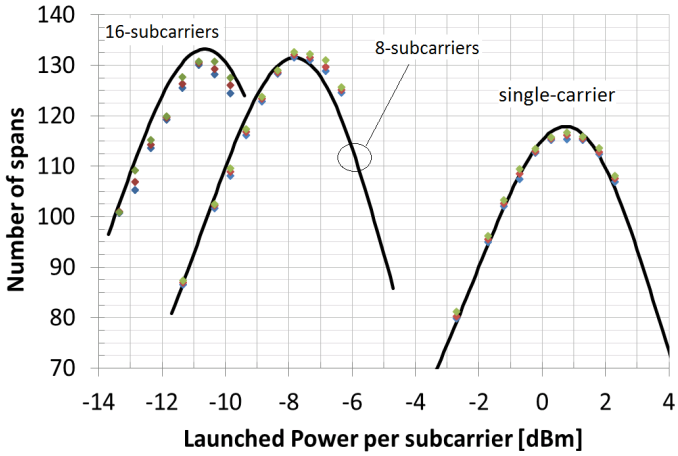

Fig. 12. Experimental results: reach in number of spans vs. power per subcarrier @ BER=10^{-2}. The system is 19-channel, PM-QPSK, 32 GBaud total per channel, 37.5 GHz channel spacing, EDFA-only, PSCF with 108 km spans. SSC: single-carrier per channel at 32 GBaud; MSC: multi-subcarrier per channel (either 8 at 4 GBaud or 16 at 2 GBaud). Markers: measurements (3 sets per launch power). Solid lines: EGN-model predictions.

hardware tuning may not be accurate enough to deal with it. We solved the problem using the discussed joint-processing of symmetric subcarriers (vs. the center channel frequency) in an 8x8 real equalizer. A forthcoming specifically-devoted paper further investigates this topic [36].

V. Comments and Conclusion

We have carried out a comprehensive study of symbol-rate-optimization (SRO). We have identified the EGN-model as a suitable tool for studying system performance optimization vs. symbol rate. The EGN-model analytical and simulative results also agree well with prior theoretical papers [1]-[6] and provide a consistent framework to reliably extend theoretical studies to a variety of scenarios.

We have shown that the max reach gain due to SRO is predicted to *increase*, when the total WDM system bandwidth goes up from a few hundred GHz to C-band. This is interesting, because other methods of non-linearity mitigation, such as digital backward-propagation (DBP) and related ones, have the opposite behavior. At C-band, SRO is predicted to substantially outperform *ideal* DBP in long-haul PM-QPSK systems using SMF (with DBP applied within the 32-GBaud channel bandwidth) and be about equivalent for PM-16QAM systems.

Overall, PM-QPSK systems with SRO could potentially achieve a max-reach increase of 10%-25%, depending on system parameters. With PM-16QAM, the potential gains are typically 60% of those with PM-QPSK.

We discussed an analytical closed-form formula predicting the optimum rate and we showed that dispersion pre-compensation may be synergistic with SRO.

We also reported on a ultra-long-haul 19-channel WDM experiment of PM-QPSK transmission, with SRO implemented through subcarrier multiplexing, that confirmed the max-reach gains predicted through the EGN model, amounting to about 13.5% vs. single-carrier for the specific set-up. We clearly identified some critical system implementation aspects which must be addressed for SRO experiments to yield their full potential.

In conclusion, we believe SRO is an effective non-linearity mitigation strategy. On the other hand, we believe its potential gains are not so strong as to make SRO *per se* a 'game-changer' in the context of high-capacity long-haul transmission. We do believe, though, that it may be one of the set of techniques that the system designers can effectively use, perhaps in combination (such as SRO and DBP together) to achieve more substantial gains.

Finally, we believe that the results that we presented may influence the general industry push towards higher symbol rates, which must be weighed vs. the greater penalties that are incurred there. In Fig. 4, the NLI gap between operating a C-band system at 32 GBaud rather than the optimum $R_{\rm opt}$=2.4 GBaud is 1.8 dB, which goes up to 2.4 dB between 96 GBaud and $R_{\rm opt}$. It grows further if the fiber used is PSCF. This means that, apart from implementation penalties, there may be a fundamental disadvantage for straight serial-rate increase. While the trend for increasing the per-carrier throughput is likely to continue, it may have to consider using some amount of electronic subcarrier multiplexing to avoid a quite substantial maximum reach penalty.

VI. Acknowledgements

This work was supported by a CISCO Sponsored Research Agreement (SRA). The authors thank SEI (Sumitomo Electric Industries) for providing the PSCF, and OCLARO for providing the Mach-Zehnder modulators, used in the experiment.

References

[1] W. Shieh and Y. Tang, 'Ultrahigh-speed signal transmission over nonlinear and dispersive fiber optic channel: the multicarrier advantage,' *IEEE Photonics J.*, vol. 2, no. 3, pp. 276-283, June 2010.

[2] C. Behrens, R. I. Killey, S. J. Savory, Ming Chen, P. Bayvel, 'Nonlinear transmission performance of higher-order modulation formats,' *IEEE Photon. Technol. Lett.*, vol. 23, no .6, pp. 377-379, Mar. 2011.

[3] L. B. Du and A. J. Lowery, 'Optimizing the subcarrier granularity of coherent optical communications systems,' *Optics Expr.*, vol. 19, no. 9, pp. 8079-8084, Apr. 2011.

[4] Q. Zhuge, B. Châtelain, D. V. Plant, 'Comparison of intra-channel nonlinearity tolerance between reduced-guard-interval CO-OFDM systems and Nyquist single carrier systems,' in *Proc. of OFC 2012*, paper OTh1B.3, Los Angeles (USA), Mar. 2012.

[5] A. Bononi, N. Rossi and P. Serena, 'Performance dependence on channel baud-rate of coherent single-carrier WDM systems,' in *Proc. of ECOC 2013*, paper Th.1.D.5, London (UK), Sept. 2013.

[6] N. Rossi, P. Serena, A. Bononi, 'Symbol-rate dependence of dominant nonlinearity and reach in coherent WDM links,' *J. of Lightw. Technol.*, vol. 33, no. 14, pp. 3132-3143, Jul. 2015.

[7] M. Qiu, Q. Zhuge, X. Xu, M. Chagnon, M. Morsy-Osman, and D. V. Plant 'Subcarrier multiplexing using DACs for fiber nonlinearity mitigation in coherent optical communication systems,' in *Proc. OFC 2014*, paper Tu3J.2, San Francisco (USA), Mar. 2014.

[8] F. Yaman, et al., 'First quasi-single-mode transmission over transoceanic distance using few-mode fibers,' in *Proc. OFC 2015*, post-deadline paper Th5C.7, Los Angeles (USA), Mar. 2015.

[9] H. Nakashima, et al., 'Experimental investigation of nonlinear tolerance of subcarrier multiplexed signals with spectrum optimization,' in *Proc. ECOC 2015*, paper Mo.3.6.4, Valencia (ES), Sept. 2015.

[10] J. Fickers, A. Ghazisaeidi, M. Salsi, G. Charlet, P. Emplit, F. Horlinet, 'Multicarrier offset-QAM for long-haul coherent optical communications,' *J. of Ligthw. Technol.*, vol. 32, no. 4, pp. 4671-4678, Dec. 2014.

[11] A. Carbo, J. Renaudier, R. Rios-Mller, P. Tran, G. Charlet, 'Experimental analysis of non linear tolerance dependency of multicarrier modulations versus bandwidth efficiency,' in *Proc. ECOC 2015*, paper Th.2.6.6, Valencia (ES), Sept. 2015.

[12] P. Poggiolini, G. Bosco, A. Carena, V. Curri, Y. Jiang, F. Forghieri, 'The GN-model of fiber non-linear propagation and its applications,' *J. of Lightw. Technol.*, vol. 32, no. 4, pp. 694-721, Feb. 2014.

[13] R. Dar, M. Feder, A. Mecozzi, M. Shtaif, 'Properties of nonlinear noise in long, dispersion-uncompensated fiber links,' *Optics Express*, vol. 21, no. 22, pp. 25685-25699, Nov. 2013.

[14] A. Carena, G. Bosco, V. Curri, Y. Jiang, P. Poggiolini and F. Forghieri, 'EGN model of non-linear fiber propagation,' *Optics Express,* vol. 22, no. 13, pp. 16335-16362, June 2014. Extended appendices with full formulas derivations can be found at *www.arXiv.org* .

[15] P. Poggiolini, Y. Jiang, A. Carena, G. Bosco, F. Forghieri, 'Analytical results on system maximum reach increase through symbol rate optimization', in *Proc. OFC 2015*, paper Th3D.6, Los Angeles (USA), Mar. 2015.

[16] P. Poggiolini, A. Carena, Y. Jiang, G. Bosco, F. Forghieri 'On the ultimate potential of symbol-rate optimization for increasing system maximum reach,' in *Proc. ECOC 2015*, paper We.4.6.2, Valencia (ES), Sept. 2015.

[17] A. Nespola, L. Bertignono, G. Bosco, A.Carena, Y. Jiang, S.M. Bilal, P. Poggiolini, S. Abrate, F. Forghieri, 'Experimental demonstration of fiber nonlinearity mitigation in a WDM multi-subcarrier coherent optical system,' in *Proc. ECOC 2015*, paper Mo.3.6.3, Valencia (ES), Sept. 2015.

[18] Amy Nordrum, 'How to thread a fiber-optic cable through the arctic,' *IEEE Spectrum*, online-only section, Jan. 2015. (http://spectrum.ieee.org/telecom/internet/how-to-thread-a-fiberoptic-cable-through-the-arctic)

[19] Corning LEAF$^{\mathrm{TM}}$, *Optical Fiber Product Information*, Jan. 2015, http://www.corning.com/WorkArea/showcontent.aspx?id=63927

[20] P. Poggiolini, G. Bosco, A. Carena, V. Curri, Y. Jiang, F. Forghieri, 'A simple and effective closed-form GN model correction formula accounting for signal non-Gaussian distribution,' *J. of Lightw. Technol.,* vol. 33, no. 2, pp. 459-473, Jan. 2015.

[21] P. Serena, A. Bononi, 'A Time-Domain Extended Gaussian Noise Model,' *J. Lightw. Technol.*, vol. 33, no. 7, pp. 1459-1472, Apr. 2015.

[22] R. Dar, M. Feder, A. Mecozzi, M. Shtaif, 'Pulse collision picture of inter-channel nonlinear interference in fiber-optic communications,' *J. Lightw. Technol.*, available at ieeexplore.ieee.org as pre-print.

[23] P. Poggiolini et al., 'Impact of low-OSNR operation on the performance of advanced coherent optical transmission systems', in *Proc. of ECOC 2014*, paper Mo.4.3.2, Cannes (FR), Sept. 2014, with corrections in the version available at www.arxiv.org, arXiv:1407.2223.

[24] P. Serena, A. Bononi, 'The nonlinear signal-noise interaction in coherent links and its implications in system design,' in *Proc. ECOC 2015*, paper We.4.6.1, Valencia (ES), Sept. 2015.

[25] V. Curri, A. Carena,P. Poggiolini, G. Bosco, F. Forghieri, 'Extension and validation of the GN model for non-linear interference to uncompensated links using Raman amplification,' *Optics Express,* vol. 21, no. 3, pp. 3308-3317, Feb. 2013.

[26] A. Carena, V. Curri, P. Poggiolini, Y. Jiang, F. Forghieri, 'Dispersion pre-compensation in PM-QPSK systems,' in *Proc. of ECOC 2014*, paper P.5.24, Cannes (FR), Sept. 2014.

[27] G. Gao, Xi Chen, W. Shieh, 'Limitation of fiber nonlinearity compensation using digital back propagation in the presence of PMD,' in *Proc. OFC 2012*, paper OM3A.5, Los Angeles (USA), Mar. 2012.

[28] M. Secondini, E. Forestieri, 'Analytical fiber-optic channel model in the presence of cross-phase modulations,' *IEEE Photon. Technol. Lett.*, vol. 24, no. 22, pp. 2016-2019, Nov. 2012.

[29] M. Secondini, E. Forestieri, G. Prati, 'Achievable information rate in nonlinear WDM fiber-optic systems with arbitrary modulation formats and dispersion maps,' *J. Lightw. Technol.*, vol. 31, no. 23, pp. 3839-3852, Dec. 2013.

[30] R. Dar, M. Feder, A. Mecozzi, and M. Shtaif, 'Accumulation of nonlinear interference noise in fiber-optic systems,' *Optics Express*, vol. 22, no. 12, pp. 14199-14211, June 2014.

[31] R. Dar, O. Geller, M. Feder, A. Mecozzi, and M. Shtaif, 'Mitigation of inter-channel nonlinear interference in WDM systems,' in Proc. of ECOC 2014, Cannes (FR), Sept. 2014.

[32] Y. Jiang, A. Carena, P. Poggiolini, F. Forghieri 'On the impact of non-linear phase-noise on the assessment of long-haul uncompensated coherent systems performance,' in Proc. of ECOC 2014, paper P.5.12, Cannes (FR), Sept. 2014.

[33] M. Secondini and E. Forestieri 'On XPM mitigation in WDM fiber-optic systems,' *IEEE Photon. Technol. Lett.*, vol. 26, no. 22, pp. 2252-2255, Nov. 2014.

[34] T. Fehenberger, N. Hanik. T. A. Eriksson, P. Johannisson, M. Karlsson, 'On the impact of carrier phase estimation on phase correlations in coherent fiber transmission,' in Proc. Tyrrhenian International Workshop on Digital Communications, TIWDC 2015, paper 3.2, Sept. 22nd 2015. (Available on IEEE Xplore)

[35] C. Schmidt-Langhorst, R. Elschner, F. Frey, R. Emmerich, C. Schubert, 'Experimental analysis of nonlinear interference noise in heterogenous flex-grid WDM transmission,' in *Proc. ECOC 2015*, paper Tu.1.4.3, Valencia (ES), Sept. 2015.

[36] G. Bosco, Syed Bilal, A. Nespola, P. Poggiolini, F. Forghieri 'Impact of the Transmitter IQ-Skew in Multi-Subcarrier Coherent Optical Systems,' in *Proc. OFC 2016*, paper W4A.5, Anaheim (USA), Mar. 2016.

[37] A. Nespola, Y. Jiang, L. Bertignono, G. Bosco, A. Carena, Syed Bilal, P. Poggiolini, F. Forghieri, 'Effectiveness of Digital Back-Propagation and Symbol-Rate Optimization in Coherent WDM Optical Systems ,' in *Proc. OFC 2016*, paper Th3D.2, Anaheim (USA), Mar. 2016.